Bifurcations of electronic trajectories and dynamics of electronic Rydberg wave packets

M. W. Beims and G. Alber
Fakultät für Physik, Albert-Ludwigs-Universität, Hermann-Herder-Strasse 3, D-7800 Freiburg im Breisgau, Germany
(Received 5 April 1993)

With the help of uniform semiclassical approximations the quantitative connection between classical bifurcation phenomena and the dynamics of an electronic Rydberg wave packet in the presence of an external static magnetic field is discussed with particular emphasis on nongeneric bifurcations of the Edmonds-Garton-Tomkins orbit.
PACS number(s): 32.60.+i, 32.80.Rm

I. INTRODUCTION

The development of short and intense laser pulses has stimulated much interest in coherent laser-induced excitation processes in which a large number of energy eigenstates of a quantum system are excited coherently and a nonstationary, localized quantum state is prepared [1]. One of the simplest physical systems in which the dynamics of such a wave packet can be studied are Rydberg atoms. Typically, a short or intense laser pulse excites coherently a large number of Rydberg states close to a photoionization threshold from an initially prepared energetically low lying bound state. Thus an electronic state is prepared which is well localized with respect to the radial electronic coordinate. The angular coordinates are still delocalized due to selection rules for radiative transitions. This radial Rydberg wave packet evolves in the Coulomb field of the positively charged ionic core. Its time evolution may be probed with the help of a typical pump-probe-type detection scheme.

From the theoretical point of view the dynamics of such a radial electronic wave packet can be described conveniently with the help of a *semiclassical path representation* [1]. Thereby the two-photon transition amplitude, which describes such a pump-probe-type experiment, is represented as a sum of contributions of all classical trajectories of a Rydberg electron. These trajectories start from and return again to the atomic core where the initial laser-induced preparation process takes place. An interesting situation arises if outside the atomic core region the dynamics of a laser-excited Rydberg electron is modified by an external static field and the corresponding classical dynamics is not integrable. In their simplest form these representations allow one to relate the quantum dynamics of the excited Rydberg electron directly to the corresponding classical dynamics in the neighborhood of *isolated closed orbits* [2–4] which start and return to the nucleus. Thus these representations yield direct quantitative insights into the connection between classical and quantum mechanics. However, the simple "isolated-closed-orbit" approach breaks down if some of the relevant classical trajectories approach each other. In this case the resulting strong quantum-mechanical interference effects between the contributions of these trajectories have not been taken into account properly. Typically, this happens at energies at which a classical bifurcation phenomenon takes place.

In this paper we study the influence of such classical bifurcation phenomena on the dynamics of an electronic wave packet in a Rydberg atom. As an example, we present results for a system which has received considerable attention recently, namely the diamagnetic Kepler problem [5–8]. Due to a discrete reflection symmetry with respect to a plane through the nucleus and perpendicular to the magnetic field, classically this problem exhibits nongeneric bifurcation phenomena. The classical dynamics of some of them has been studied by Mao and Delos [9] recently. An interesting example is the period-4 bifurcation of the Edmonds-Garton-Tomkins orbit which extends along a straight line through the nucleus in the symmetry plane. Using uniform semiclassical methods [10, 11] semiclassical path representations are derived for the two-photon transition amplitude which describes a typical pump-probe-type experiment where the dynamics of an electronic Rydberg wave packet is probed. This way quantitative insight into the relation between these classical bifurcation phenomena and the quantum dynamics of an electronic Rydberg wave packet which moves under the influence of the Coulomb potential of the positively charged ionic core and the external static magnetic field is obtained.

The paper is organized as follows. In Sec. II a summary of results on the semiclassical path representation of two-photon transition amplitudes which describe pump-probe-type experiments is given. In Sec. III a uniform semiclassical path representation is derived for this two-photon transition amplitude which describes the short-time behavior of an electronic Rydberg wave packet in the energy regime where nongeneric bifurcation phenomena of the Edmonds-Garton-Tomkins orbit take place.

II. BASIC EQUATIONS

In this section previously derived results on the semiclassical path representation of the two-photon transition

amplitude [1] which describes pump-probe-type experiments for a Rydberg atom in a weak static magnetic field are summarized.

A quantity of central importance in the description of atomic processes which involve the absorption and stimulated emission of laser radiation is the resonant part of the two-photon transition amplitude. For a transition between initial and final atomic states $\mid g\rangle$ and $\mid f\rangle$ it is given by (see Fig. 1) [1]

$$T_{fg}(\varepsilon) = \langle f \mid \boldsymbol{\mu}\cdot\boldsymbol{\epsilon}_2^*(\varepsilon - H + i0)^{-1}\boldsymbol{\mu}\cdot\boldsymbol{\epsilon}_1 \mid g\rangle \qquad (\varepsilon \approx \varepsilon_g + \omega_1 \approx \varepsilon_f + \omega_2). \quad (1)$$

Thereby the Hamiltonian

$$H = H_A - \gamma L_z + \tfrac{1}{2}\gamma^2 r^2 \sin^2\theta \quad (2)$$

describes the dynamics of an excited valence electron with polar coordinates (r,θ,φ) in the presence of a uniform, static magnetic field. The atomic Hamiltonian is denoted H_A and L_z is the angular momentum in the direction of the magnetic field whose field strength γ is measured in units of $B_0 = 4.72\times 10^5$ T. The atomic dipole operator is denoted $\boldsymbol{\mu}$ and $\boldsymbol{\epsilon}_{1(2)}$, $\omega_{1(2)}$ are polarization and frequency of the absorbed (emitted) laser radiation. With the replacement $\boldsymbol{\epsilon}_2^* \to \boldsymbol{\epsilon}_2$ Eq. (1) describes also one-photon resonant two-photon absorption. In terms of the matrix element $T_{fg}(\varepsilon)$ the transition probability between initial and final states $\mid g\rangle$ and $\mid f\rangle$ of a typical pump-probe-type experiment with two nonoverlapping time-delayed short laser pulses is given by

$$P_{g\to f} = \left| \frac{1}{2\pi}\int_{-\infty}^{\infty} d\varepsilon\, e^{-i\varepsilon(t_2-t_1)} T_{fg}(\varepsilon)\tilde{\mathcal{E}}_1(\varepsilon-\varepsilon_g-\omega_1) \times \tilde{\mathcal{E}}_2^*(\varepsilon-\varepsilon_f-\omega_2)\right|^2, \quad (3)$$

with $\tilde{\mathcal{E}}_i(\varepsilon) = \int_{-\infty}^{\infty} dt\, e^{i\varepsilon t}\mathcal{E}_i(t+t_i)$ denoting the Fourier transform of the laser fields $\mathbf{E}_i(t) = \mathcal{E}_i(t)\mathbf{e}_i e^{-i\omega_i t}$ + c.c. $(i=1,2)$. The slowly varying envelopes of the laser pulses $\mathcal{E}_{1,2}(t)$ are assumed to be centered around times t_1 and t_2 with pulse durations τ_1 and τ_2 ($\tau_{1,2} \ll t_2 - t_1$). Furthermore, accoording to Fermi's golden rule the time-independent photoabsorption rate

$$\Gamma = -2\,\mathrm{Im}[T_{gg} \mid \mathcal{E} \mid^2]_{\varepsilon=\varepsilon_g+\omega} \quad (4)$$

describes resonant excitation by a weak and long laser pulse from an initial state $\mid g\rangle$.

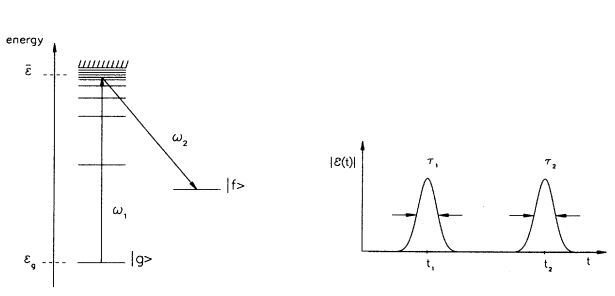

FIG. 1. Schematic representation of a pump-probe experiment with two time delayed short laser pulses.

In cases in which the dynamics of an excited valence electron in the presence of a static external field is modified significantly only at large distances from the nucleus, in general three characteristic spatial regimes may be distinguished.

(1) The atom-laser interaction as well as electron correlation effects are localized in a *reaction zone* which typically extends only a few Bohr radii around the atomic nucleus.

(2) In the surrounding *Coulomb zone* the dynamics of a highly excited Rydberg electron is determined dominantly by the Coulomb potential of the positively charged ionic core.

(3) At sufficiently large distances from the atomic nucleus, i.e., in the *asymptotic zone*, the static external field becomes at least as important as the Coulomb potential.

If the applied static external field is sufficiently weak the extension of the Coulomb zone is large in comparison with the Bohr radius which implies relevant classical action much larger than $\hbar$. Based on this observation *a semiclassical path representation* may be derived for the two-photon transition amplitude by combining semiclassical methods with methods of quantum defect theory. Thereby this quantity is expressed as a sum of probability amplitudes of all classical trajectories which leave the Coulomb zone with pure radial momentum and return again to the reaction zone. In the absence of an external field the rotational symmetry of the Coulomb problem implies that all trajectories return again to the reaction zone with the same value of the classical action thus interfering constructively. In this limit the semiclassical path representation reduces to the well-known results of quantum defect theory. In the case of a weak external static magnetic field, i.e., $\gamma \ll 1$, it is found that [1]

$$T_{fi}(\varepsilon) = T_{fi}^{(s)} + (2\pi)^{5/2}\sum_{j,n_j}\sum_m d_m^+(\theta_j) d_m^-(\theta_{0j}) \times [\sigma_j^{(n_j)}]^{1/2} e^{i[n_j S_j - m n_j \pi\nu_j - \mu_{n_j}\pi/2+\pi/4]}\,|_{\varepsilon_m}\,. \quad (5)$$

All quantities in Eq. (5) have to be evaluated at energy $\varepsilon_m = \varepsilon + m\gamma$ with the magnetic quantum number m. Thereby the two-photon transition amplitude is expressed as a sum of contributions of all *isolated closed orbits* j, which start from and return again to the atomic nucleus with angles θ_{0j} and θ_j. The integer n_j counts the number of traversals of these orbits. The probability amplitude of the n_jth return of orbit j to the reaction zone is determined by the following.

(1) Photoionization and recombination dipole matrix elements [1], i.e.,

$$d_m^{(-)}(\theta_{0j}) = \sum_l \mathcal{D}_{lm}^{(-)}(-1)^l Y_l^m(\theta_{0j},0) \quad (6)$$

and

$$d_m^{(+)}(\theta_j) = \sum_l \mathcal{D}_{lm}^{(+)}(-1)^l Y_l^m(\theta_j,0)^* \quad (7)$$

(they characterize the atom-laser interaction and possible

electron-correlation effects inside the reaction zone).

(2) The classical action, $n_j S_j$, the Maslov index, μ_{n_j}, the number of crossings of the symmetry axis $n_j \nu_j$, and the cross section

$$\sigma_j^{(n_j)} = \frac{\sin\theta_j \sin\theta_{0j}}{\left| \frac{\partial p_\theta}{\partial \theta_0} \frac{\sin(n_j u_j)}{\sin(u_j)} \right|_j}, \tag{8}$$

which characterize the classical motion of the excited Rydberg electron in the Coulomb field of the positively charged ionic core and the external magnetic field.

Due to the axial symmetry of the diamagnetic Kepler problem around the magnetic field axis the contributing closed orbits form one-parameter families with respect to the angular coordinate φ and are only isolated with respect to the angular coordinate θ. All orbits within such a family, i.e., with different emission angles φ_0, interfere constructively. The cross section $\sigma_j^{(n_j)}$ determines the range of initial emission angles $\Delta\theta_{0j}$ within which orbits interfere constructively (Fresnel zone) [12]. It is determined by the derivative of the angular momentum p_θ with respect to θ_0. Scaling properties of the Hamiltonian of Eq. (2) imply that classical actions of closed orbits are proportional to $\lambda = \gamma^{-1/3}$ (in units of $\hbar$) so that $\sigma_j^{(n_j)} = O(\lambda^{-1})$ and the extension of the Fresnel zone tends to zero in the semiclassical limit $\lambda \gg 1$. The quantity u_j is the imaginary part of the stability exponent of the closed orbit j. The first term in Eq. (5), $T_{fg}^{(s)}$, describes the "direct" part of the two-photon amplitude and is approximately energy independent. In the absence of any closed orbits it is the only contribution to T_{fg}. It should be mentioned that in practical applications of Eq. (5) typically only closed trajectories with orbit times $T_j < T_{\max}$ are taken into account. Thereby $T_{\max}$ is a typical observation time of interest. This amounts to an averaging of $T_{fg}(\varepsilon)$ over an energy interval of the order of $\Delta\varepsilon \approx 2\pi/T_{\max}$.

As a major approximation in the derivation of Eq. (5) it has been assumed that the contributions of all relevant (families of) closed orbits are well separated spatially. This assumption breaks down if contributing (families of) orbits approach each other and the corresponding Fresnel zones of initial angles start to overlap. This may happen at particular energies whenever a classical bifurcation phenomenon takes place and

$$\frac{\partial p_\theta}{\partial \theta_0}_j \sin(n_j u_j) = 0 \tag{9}$$

for the contribution of the n_jth return of an electron along a closed orbit j. This implies that $\sigma_j^{(n_j)} \to \infty$. In this case the contribution of overlapping trajectories, for example $\{(j_1, n_{j1}), (j_2, n_{j2}), \ldots, (j_N, n_{jN})\}$, to the two-photon transition amplitude may be determined by using uniform semiclassical approximation techniques [10, 11]. A comparison integral with which, for a given value of the magnetic quantum number m, the contributions of these N (families of) closed orbits can be described in a uniform way is given by

$$J_{Nm}(\varepsilon) = \int_0^\pi d\theta_0 G_{Nm}(\theta_0, \varepsilon) e^{iF_{N+1}(\theta_0, \varepsilon)}, \tag{10}$$

with $F_{N+1}(\theta_0, \varepsilon)$ and $G_{Nm}(\theta_0, \varepsilon)$ denoting polynomials of degrees $(N+1)$ and N. The coefficients of these polynomials may be determined by the requirements that the stationary phase points of this uniform integral are identical with the emission angles of the relevant classical trajectories. Further, one requires that in the semiclassical limit, i.e., $\lambda = \gamma^{-1/3} \gg 1$, for energies sufficiently far away from the bifurcation energy the stationary phase evaluation of $J_{Nm}(\varepsilon)$ reduces to the corresponding result of the "isolated orbit approximation" as given in Eq. (5).

III. APPLICATION

In this section the "isolated-closed-orbit" representation of $T_{fg}(\varepsilon)$ as given in Eq. (5) is generalized to a description of bifurcation phenomena in the diamagnetic Kepler problem with particular emphasis on bifurcations of period 4, period 7, and period 18 of the Edmonds-Garton-Tomkins orbit.

The classical mechanics of bifurcation phenomena which occur in the diamagnetic Kepler problem has been discussed recently by Mao and Delos [9]. In particular, it has been shown that, due to the discrete reflection symmetry of the Hamiltonian with respect to a plane through the Coulomb center perpendicular to the magnetic field axis, nongeneric bifurcation phenomena take place. An interesting case is the period-4 bifurcation of the periodic Edmonds-Garton-Tomkins orbit I_0 (with classical orbit time T_0) whose path starts from the Coulomb center and extends on a straight line in the symmetry plane perpendicular to the magnetic field axis. Due to this reflection symmetry at energy $\varepsilon_1 = -0.503\,75\gamma^{2/3}$ a saddle-node bifurcation leads to the creation of a stable and unstable closed orbit (I_1, I_2) and the reflected counterpart (I_{-1}, I_{-2}). Both pairs of orbits are located close to the periodic orbit I_0 and return to the nucleus approximately at even multiples of the classical orbit time T_0. At energy $\varepsilon_2 = -0.501\,91\gamma^{2/3}$ the stable orbit I_1 and its reflected counterpart I_{-1} coalesce with the periodic orbit I_0 and for energies $\varepsilon > \varepsilon_2$ only the unstable closed orbit I_2 and its counterpart I_{-2} together with orbit I_0 remain. In Fig. 2(a) the emission angles θ_0 of these closed orbits are shown as a function of scaled energy $\tilde{\varepsilon} = \varepsilon/\gamma^{2/3}$. The form of these orbits is depicted in Fig. 2(b).

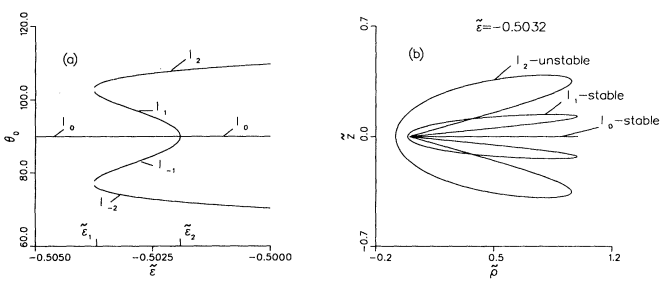

FIG. 2. Initial starting angles θ_0 of orbits I_0,$I_{\pm1}$,$I_{\pm2}$ as a function of scaled energy $\tilde{\varepsilon} = \varepsilon/\gamma^{2/3}$ (a) and their form (b) with $\tilde{\rho} = \sqrt{x^2 + y^2}\gamma^{2/3}$ and $\tilde{z} = z\gamma^{2/3}$.

In the energy range $\varepsilon \approx \varepsilon_1 \approx \varepsilon_2$ and for a given value of the magnetic quantum number m the contributions of the five closed orbits (I_s, n_s) with $(s = 0, \pm 1, \pm 2)$ and $n_{\pm 1} = n_{\pm 2} = 1$, $n_0 = 2 \equiv n$, for example, to the two-photon transition amplitude can be described with the help of the comparison integral of a cuspoidal butterfly catastrophe [13],

$$J_{5m}^{(n)}(\varepsilon) = \int_{-\infty}^{\infty} d\theta_0 G_{5m}^{(n)}(\theta_0, \varepsilon) e^{iF_6^{(n)}(\theta_0, \varepsilon)}, \tag{11}$$

with the polynomials

$$G_{5m}^{(n)}(\theta_0, \varepsilon) = \sum_{k=0,1,2} A_{km}^{(n)}(\varepsilon)(\theta_0 - \pi/2)^{2k} \tag{12}$$

and

$$F_6^{(n)}(\theta_0, \varepsilon) = \sum_{k=0,1,2,3} a_k^{(n)}(\varepsilon)(\theta_0 - \pi/2)^{2k}. \tag{13}$$

In Eq. (11) we have assumed that the main contribution to the integral comes from angles $\theta_0 \approx \pi/2$ so that the limits of integration may be extended to infinity. The special form of these polynomials already take into account the reflection symmetry of the diamagnetic Kepler problem. As shown in the Appendix, in the energy regime $\varepsilon_1 < \varepsilon < \varepsilon_2$ the parameters of these polynomials are determined by the classical properties of the relevant five closed orbits by the requirement that Eq. (11) has to reduce to the corresponding part of the "closed-orbit representation" as given in Eq. (5) for $\lambda \gg 1$ and for energies sufficiently far away from the bifurcation energies. These parameters are slowly varying functions of energy across the bifurcation region. Their relation to the dipole matrix elements and classical properties of the relevant trajectories which appear in Eq. (5) are summarized in the Appendix. Similar bifurcation phenomena of period 7 and period 18 take place around energies $\varepsilon_3 = -0.4194\gamma^{2/3}$ and $\varepsilon_4 = -0.4365\gamma^{2/3}$. In Fig. 3 the energy dependence of $\sin(n_0 u_0)$ is shown. According to Eq. (9) whenever this quantity tends to zero the "isolated-closed-orbit" representation of Eq. (5) breaks down and a bifurcation phenomenon which involves the Edmonds-Garton-Tomkins orbit I_0 takes place. Figure 3 shows that as far as contributions with $n_0 \leq 10$ are concerned these are the only bifurcation phenomena of orbit I_0 which take place in the energy regime $-0.55 < \tilde{\varepsilon} < -0.4$. The form of the stable and unstable periodic orbits which are involved in the bifurcations at energies ε_4 and ε_3 are shown in Fig. 4.

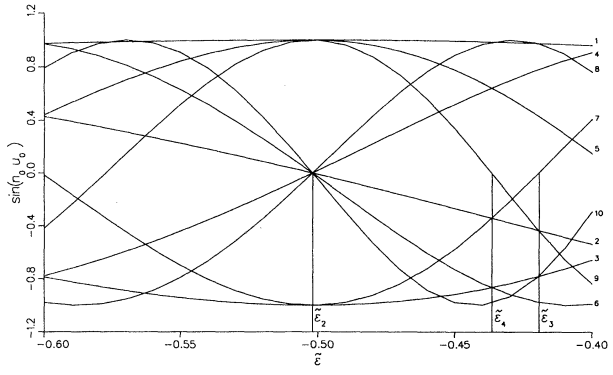

FIG. 3. Energy dependence of $\sin(n_0 u_0)$ with the imaginary part of the stability exponent u_0 of orbit I_0.

The influence of these classical bifurcation phenomena on the time evolution of an electronic wave packet may be studied with the help of a pump-probe-type experiment [1]. Thereby a first short laser pulse centered around time t_1 (pulse duration τ_1, frequency ω_1, and polarization $\mathbf{e}_1$) prepares a radial electronic wave packet by exciting a large number of atomic Rydberg states coherently from an initially prepared energetically low-lying bound state. As soon as this electronic wave packet leaves the Coulomb zone it is split into various fractions by the combined action of the Coulomb and external magnetic field. These various fractions return to the reaction zone at different times thereby moving along one of the classical closed orbits. They may be probed by a second short laser pulse centered at time t_2 (pulse duration τ_2, frequency ω_2, and polarization $\mathbf{e}_2$) which induces an atomic transition to some energetically low-lying bound state or to continuum states well above the photoionization threshold after a time delay $\Delta t = t_2 - t_1$. The probability of finding the atom in the final state is large whenever the time delay between both laser pulses is a multiple of one of the classical orbit times of the closed orbits. By changing the polarizations and frequencies of pump and probe pulse the relevant emission angles and the mean excited energy of the generated electronic wave packet may be varied. Thus, for example, choosing the polarizations of pump and probe pulse orthogonal to the magnetic field axis, an excited Rydberg electron is emitted from the reaction zone dominantly with $\theta_0 \approx \pi/2$ and is probed by the second laser pulse if it returns again with $\theta \approx \pi/2$. In this case the two-photon transition amplitude may be approximated uniformly by

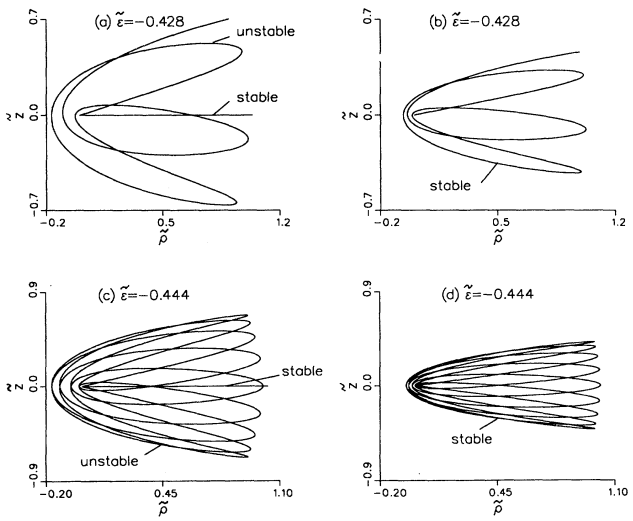

FIG. 4. Unstable and stable orbits involved in the bifurcations of periods 7 and 18 which take place at energies ε_4 [(a) and (b)] and ε_3 [(c) and (d)].

$$T_{fg}(\varepsilon) = T_{fg}^{(s)} + \sum_{m=\pm1} \Bigg\{ \sum_{n=2,4,6,8,10} J_{5m}^{(n)}(\varepsilon_m) + J_{5m}^{(7)}(\varepsilon_m) + J_{5m}^{(9)}(\varepsilon_m) \Bigg\}$$

$$+ (2\pi)^{5/2} \sum_{n=1,3,5} \sum_{m} d_m^{+}(\pi/2) d_m^{-}(\pi/2) [\sigma_j^{(n)}]^{1/2} \times e^{i[nS_0 - (3+7(n-1)/2)\pi/2 + \pi/4]} \mid_{\varepsilon_m}, \quad (14)$$

as long as the significantly excited range of scaled energies lies within the interval $(-0.55, -0.4)$ and the relevant observation time $\Delta t = t_2 - t_1$ is less than $T_{\max} = 10T_0$. Inserting Eq. (14) into Eq. (3) we obtain the probability of finding the atom in the final state $|f\rangle$ after the interaction with both laser pulses.

Figures 5 and 6 show the final-state probability which describes the result of a pump-probe experiment. For simplicity, results are shown for hydrogen, though nonhydrogenic core effects might be taken into account in a straightforward way [4, 14]. The laser polarization of pump and probe pulse are both perpendicular to the magnetic field, so that the excited Rydberg electron is emitted predominantly orthogonal to the magnetic field. The envelopes of the laser pulses are assumed to be Gaussian, i.e., $\mathcal{E}_{1,2}(t) = \mathcal{E}_0 \exp[-(t - t_{1,2})^2/(2\tau^2)]$. For simplicity we also assume that the initially prepared atomic state is an s state and that the initial and final state are identical. In this case we have the relation

$$2\pi \mathcal{D}_{l=1m=\pm1}^{(+)} \mathcal{D}_{l=1m=\pm1}^{(-)} \mid \mathcal{E}_0 \mid^2 = -\tfrac{1}{2}\Gamma.$$

The quantity Γ is the photoionization rate which according to Fermi's golden rule describes excitation of continuum states at threshold in the absence of a magnetic field. For the sake of completeness the energy dependence of the coefficients which according to Eqs. (12) and (13) determine the uniform comparison integrals of Eq. (14) are summarized in Table I. The corresponding pump-probe transition probability has been evaluated numerically from Eqs. (14) and (3).

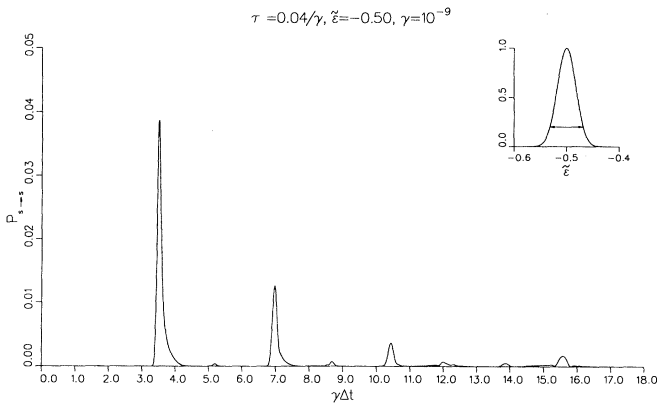

FIG. 5. Two-photon transition probability of a pump-probe experiment in units of $(\Gamma\tau)^2$ with $\bar{\varepsilon} = \varepsilon_g + \omega_1 = \varepsilon_f + \omega_2 = -0.50\gamma^{2/3}$, $\gamma = 10^{-9}$, and pulse duration $\tau = 0.04/\gamma$.

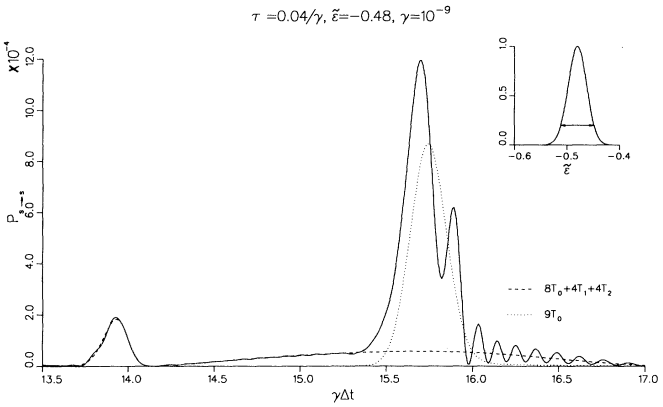

FIG. 6. Two-photon transition probability in units of $(\Gamma\tau)^2$ with $\bar{\varepsilon} = \varepsilon_g + \omega_1 = \varepsilon_f + \omega_2 = -0.48\gamma^{2/3}$ and all other parameters as in Fig. 5.

In Fig. 5 the final-state probability is shown as a function of the time delay $\Delta t = t_2 - t_1$ between pump and probe pulse. The recombination peaks at multiples of the orbit time $T_0 \approx 1.7/\gamma$ of the Edmonds-Garton-Tomkins orbit I_0 correspond to repeated returns of fractions of the initially prepared electronic wave packet to the atomic core region. During their returns these fractions are localized around orbit I_0. In the energy region which is excited significantly by the first laser pulse and which is centered around energy $\bar{\varepsilon} = -0.5\gamma^{2/3}$, classical bifurcation phenomena take place. The inset in the right upper corner of Fig. 5 shows the energy dependence of the Fourier transform of the slowly varying envelopes of the laser pulses. The large maxima at even multiples of T_0 in the main part of Fig. 5 are due to strong quantum-mechanical interferences between the probability amplitudes of the bifurcating classical orbits whose form is shown in Fig. 2(b). The time dependence of these recombination peaks exhibits asymmetric structures whose widths are much larger than the pulse durations τ of pump and probe pulse. These large widths reflect the fact that in the energy regime in which a classical bifurcation phenomenon takes place the orbit times of the orbits involved depend strongly on energy. Therefore the significantly excited energy regime, i.e., $(\bar{\varepsilon} - 1/\tau, \bar{\varepsilon} + 1/\tau)$, leads to a large spreading of the return times of the returning fractions of the initially prepared electronic wave packet.

In Fig. 6 the typical structure of the recombination peaks is shown in more detail. The time delays between pump and probe pulse include time delays between $8T_0$ and $9T_0$ and the mean excited energy lies slightly above the bifurcation energy ε_2. The energy regime which is excited significantly by the first laser pulse is indicated by the arrow in the inset in the right upper corner of Fig. 6. The corresponding spreadings of the relevant return times of the closed classical orbits $I_0, I_{\pm1}$, and $I_{\pm2}$, i.e., $8T_0, 9T_0$, $4T_1$, and $4T_2$, are also indicated by arrows. The full curve shows the result of the calculation based on Eqs. (3) and (14). Thereby all quantum-mechanical interference effects between contributions of different orbits have been taken into account properly. The first recombination peak around $\Delta t \approx 13.9/\gamma$ originates predomi-

nantly from a fraction of the initially prepared electronic wave packet which has evolved along the periodic orbit I_0 for eight periods. The adjacent broad peak is due to fractions of the electronic wave packet which have evolved along the bifurcated orbits $I_{\pm 2}$ for two periods, i.e,. $4T_2$. The recombination peak at $\Delta t \approx 15.7/\gamma$ originates predominantly from a fraction of the electronic wave packet which has evolved along the Edmonds-Garton-Tomkins orbit I_0 for nine periods. The corresponding probability of this contribution only is shown by the dotted curve in Fig. 6. The dashed curve in Fig. 6 shows the final-state probability without this contribution. The significantly excited energy regime includes also energy ε_4 around which a bifurcation phenomenon of period-18 takes place. The stable and unstable closed orbits which are involved in this bifurcation phenomenon are shown in Figs. 4(c) and 4(d). Due to quantum-mechanical interferences the recombination peak of these bifurcating orbits alone, i.e., the dotted curve of Fig. 6, exhibits an asymmetric line shape. Comparing the dashed and dotted curves it is apparent that the oscillations of the full curve of Fig. 6 for time delays $\Delta t > 15.9/\gamma$ are due to quantum-mechanical interferences between the probability amplitudes of the unstable orbits which are generated in the classical bifurcation phenomena of period 4 and period 18 and whose form is shown in Figs. 2(b) and 4(c).

In conclusion, we have shown that with the help of uniform *semiclassical path representations* of relevant atomic transition probability amplitudes typical pump-probe-type experiments in which the dynamcis of an electronic wave packet is investigated can be described even in cases in which classical bifurcation phenomena take place. This approach allows one to connect the classical aspects of these bifurcation phenomena quantitatively in a straightforward way with the quantum-mechanical time evolution of the laser-prepared electronic wave packet.

ACKNOWLEDGMENTS

This work was supported by the SFB 276 of the Deutsche Forschungsgemeinschaft and the Deutsche Akademische Austauschdienst.

APPENDIX

For the uniform semiclassical description [10, 11] of the contributions of orbits (I_s, n_s) to the two-photon transition amplitude of Eq. (5) with $s = 0, \pm 1, \pm 2$, $2n_{\pm 1} = 2n_{\pm 2} = n_0 \equiv n$ and a given value of the magnetic quantum number m we start from the comparison integral $J_{5m}^{(n)}(\varepsilon)$ of Eq. (11). The five saddle points of the polynomial $F_6^{(n)}(\theta_0, \varepsilon)$ are given by

TABLE I. Polynomial fits of parameters entering uniform integrals of Eq. (14) for $m = \pm 1$ with $\Delta\tilde{\varepsilon}_2 = \tilde{\varepsilon} - \tilde{\varepsilon}_2$, $\Delta\tilde{\varepsilon}_7 = \tilde{\varepsilon} - \tilde{\varepsilon}_3$ and $\Delta\tilde{\varepsilon}_9 = \tilde{\varepsilon} - \tilde{\varepsilon}_4$; furthermore $A_{0m}^{(n)} e^{-i[-7(n/2)(\pi/2)+\pi/2]}/(\Gamma/2) = [0.7829 - 0.5767\Delta\tilde{\varepsilon}_2 + 0.090197\Delta\tilde{\varepsilon}_2^2]\sqrt{(n/2)\sin(2u_0)/\sin(nu_0)}$ for $n = 2, 4, 6, 8, 10$, $A_{0m}^{(7)} e^{-i[-24(\pi/2)+\pi/2]}/(\Gamma/2) = [0.7654 - 0.6127\Delta\tilde{\varepsilon}_7 + 27.27931\Delta\tilde{\varepsilon}_7^2]$ for $n = 7$, and $A_{0m}^{(9)} e^{-i[-31(\pi/2)+\pi/2]}/(\Gamma/2) = [0.7548 - 0.3505\Delta\tilde{\varepsilon}_9 + 42.59304\Delta\tilde{\varepsilon}_9^2]$ for $n = 9$.

	n=2,4,6,8,10
$a_0^{(n)}\gamma^{1/3}$	$n[4.81932 + 1.72917\Delta\tilde{\varepsilon}_2 + 0.404900\Delta\tilde{\varepsilon}_2^2]$ (valid also for n=7,9)
$a_1^{(n)}\gamma^{1/3}$	$(n/2)[3.64531\Delta\tilde{\varepsilon}_2 + 4.3475\Delta\tilde{\varepsilon}_2^2]$
$a_2^{(n)}\gamma^{1/3}$	$(n/2)[0.12806 + 1.68839\Delta\tilde{\varepsilon}_2 + 57.0401\Delta\tilde{\varepsilon}_2^2]$
$a_3^{(n)}\gamma^{1/3}$	$(n/2)[-0.897465 - 13.9418\Delta\tilde{\varepsilon}_2 - 118.585\Delta\tilde{\varepsilon}_2^2]$

	n=7
$a_1^{(7)}\gamma^{1/3}$	$17.2791\Delta\tilde{\varepsilon}_7 + 34.8845\Delta\tilde{\varepsilon}_7^2$
$a_2^{(7)}\gamma^{1/3}$	$2.01800 + 6.92242\Delta\tilde{\varepsilon}_7 + 55.1622\Delta\tilde{\varepsilon}_7^2$
$a_3^{(7)}\gamma^{1/3}$	$-7.22128 - 48.4066\Delta\tilde{\varepsilon}_7 - 377.328\Delta\tilde{\varepsilon}_7^2$

	n=9
$a_1^{(9)}\gamma^{1/3}$	$19.3214\Delta\tilde{\varepsilon}_9 - 6.88528\Delta\tilde{\varepsilon}_9^2$
$a_2^{(9)}\gamma^{1/3}$	$2.05444 + 14.7159\Delta\tilde{\varepsilon}_9 + 481.593\Delta\tilde{\varepsilon}_9^2$
$a_3^{(9)}\gamma^{1/3}$	$-7.27442 - 68.0996\Delta\tilde{\varepsilon}_9 - 1169.93\Delta\tilde{\varepsilon}_9^2$

n	$A_{1m}^{(n)} e^{-i[-7(n/2)(\pi/2)+\pi/2]}/(-\Gamma/2)$	$A_{2m}^{(n)} e^{-i[-7(n/2)(\pi/2)+\pi/2]}/(-\Gamma/2)$
2	$1.91009 + 4.82352\Delta\tilde{\varepsilon}_2$	$-2.77874 - 11.6394\Delta\tilde{\varepsilon}_2$
4	$1.90955 + 8.21149\Delta\tilde{\varepsilon}_2$	$-2.63547 - 6.15000\Delta\tilde{\varepsilon}_2$
6	$1.90954 + 13.9209\Delta\tilde{\varepsilon}_2$	$-2.39696 - 3.06552\Delta\tilde{\varepsilon}_2$
8	$1.90953 + 21.914\Delta\tilde{\varepsilon}_2$	$-2.06434 + 15.9449\Delta\tilde{\varepsilon}_2$
10	$1.90954 + 32.191\Delta\tilde{\varepsilon}_2$	$-1.64413 - 26.2375\Delta\tilde{\varepsilon}_2$
7	$A_{1m}^{(7)} e^{-i[-24(\pi/2)+\pi/2]}/(-\Gamma/2) =$ $1.8046 - 9.5159\Delta\tilde{\varepsilon}_7$	$A_{2m}^{(7)} e^{-i[-24(\pi/2)+\pi/2]}/(-\Gamma/2) =$ $-5.96347 + 7.50162\Delta\tilde{\varepsilon}_7 + 152.8735\Delta\tilde{\varepsilon}_7^2$
9	$A_{1m}^{(9)} e^{-i[-31(\pi/2)+\pi/2]}/(-\Gamma/2) =$ $1.55491 - 13.24845\Delta\tilde{\varepsilon}_9$	$A_{2m}^{(9)} e^{-i[-31(\pi/2)+\pi/2]}/(-\Gamma/2) =$ $-4.89546 + 20.8087\Delta\tilde{\varepsilon}_9$

$$X_s = \begin{cases} 0 & (s=0) \\ \pm\left[-\frac{a_2(\varepsilon)}{3a_3(\varepsilon)} + \sqrt{\left(\frac{a_2(\varepsilon)}{3a_3(\varepsilon)}\right)^2 - \frac{a_1(\varepsilon)}{3a_3(\varepsilon)}}\right]^{1/2} & (s=\pm 1) \\ \pm\left[-\frac{a_2(\varepsilon)}{3a_3(\varepsilon)} - \sqrt{\left(\frac{a_2(\varepsilon)}{3a_3(\varepsilon)}\right)^2 - \frac{a_1(\varepsilon)}{3a_3(\varepsilon)}}\right]^{1/2} & (s=\pm 2), \end{cases}$$

with $X_s = \theta_{0s} - \pi/2$ and $(s = 0, \pm 1, \pm 2)$. For simplicity of notation we have suppressed the superscript (n) in the coefficients $a_k^{(n)}(\varepsilon)$. The corresponding second derivatives are given by

$$\left.\frac{\partial^2 F_6^{(n)}}{\partial \theta_0^2}\right|_{X_s} = \begin{cases} 2a_1(\varepsilon) & (s=0) \\ 2[a_1(\varepsilon) + 6a_2(\varepsilon)X_s^2 + 15a_3(\varepsilon)X_s^4] & (s=\pm 1, \pm 2). \end{cases}$$

In the energy regime $\varepsilon_1 < \varepsilon < \varepsilon_2$ the saddle points θ_{0s} with $(s = 0, \pm 1, \pm 2)$ are required to be real valued and are identified with the emission angles of the corresponding orbits I_s with $(s = 0, \pm 1, \pm 2)$. Furthermore, the corresponding classical actions $S_s(\varepsilon)$ are set equal to $F_6^{(n)}(\theta_{0s}, \varepsilon)$. This implies the relations

$$\begin{aligned} a_0(\varepsilon) &= S_0(\varepsilon), \\ a_1(\varepsilon) &= 3a_3(\varepsilon)(\theta_{01} - \pi/2)^2(\theta_{02} - \pi/2)^2, \\ a_2(\varepsilon) &= -\frac{3a_3(\varepsilon)}{2}[(\theta_{01} - \pi/2)^2 + (\theta_{02} - \pi/2)^2], \\ a_3(\varepsilon) &= \frac{n[S_1(\varepsilon) - S_2(\varepsilon)]}{[(\theta_{02} - \pi/2)^2 - (\theta_{01} - \pi/2)^2]^3}, \end{aligned} \tag{A1}$$

which determine the energy dependence of the coefficients of the polynomial $F_6^{(n)}(\theta_0, \varepsilon)$ in this energy regime. As these coefficients are smooth functions of energy across the bifurcation energies ε_1 and ε_2 they can be extrapolated easily with the help of polynomial fits with respect to energy.

The energy dependence of the coefficients of the polynomial $G_{5m}^{(n)}(\theta_0, \varepsilon)$ are determined by the requirement that in the energy regime $\varepsilon_1 < \varepsilon < \varepsilon_2$ in the semiclassical limit, i.e., $\lambda = \gamma^{-1/3} \gg 1$, the uniform comparison integral $J_{5m}^{(n)}(\varepsilon)$ should reduce to the corresponding "isolated-closed-orbit" contributions of orbits $I_s (s = 0, \pm 1, \pm 2)$ as given in Eq. (5). This implies the relations

$$G_{5m}^{(n)}(\theta_{0s}, \varepsilon) = d_m^{(+)}(\theta_s) d_m^{(-)}(\theta_{0s}) e^{-im n_s \pi \nu_s} (2\pi)^2 \left[\sigma_s^{(n_s)} \left|\frac{\partial^2 F_6^{(n)}}{\partial \theta_{0s}^2}\right|\right]^{1/2} e^{i[-\mu_{n_s}\pi/2 + \pi/4 - \mathrm{sgn}(\partial^2 F_6^{(n)}/\partial\theta_{0s}^2)\pi/4]} \tag{A2}$$

for $(s = 0, \pm 1, \pm 2)$ and

$$\begin{aligned} A_{0m}(\varepsilon) &= G_{5m}^{(n)}(\theta_{00}, \varepsilon), \\ A_{1m}(\varepsilon) &= \frac{[G_{5m}^{(n)}(\theta_{00}, \varepsilon) - G_{5m}^{(n)}(\theta_{02}, \varepsilon)]X_1^2}{X_2^2(X_2^2 - X_1^2)} - \frac{[G_{5m}^{(n)}(\theta_{00}, \varepsilon) - G_{5m}^{(n)}(\theta_{01}, \varepsilon)]X_2^2}{X_1^2(X_2^2 - X_1^2)}, \\ A_{2m}(\varepsilon) &= \frac{[G_{5m}^{(n)}(\theta_{02}, \varepsilon) - G_{5m}^{(n)}(\theta_{00}, \varepsilon)]}{X_2^2(X_2^2 - X_1^2)} - \frac{[G_{5m}^{(n)}(\theta_{01}, \varepsilon) - G_{5m}^{(n)}(\theta_{00}, \varepsilon)]}{X_1^2(X_2^2 - X_1^2)}. \end{aligned} \tag{A3}$$

Again these quantities are slowly varying functions of energy across the bifurcation energies and can be extrapolated beyond this energy regime by polynomial fits with respect to energy.

[1] G. Alber and P. Zoller, Phys. Rep. **199**, 231 (1991).
[2] E.B. Bogomolny, Pis'ma Zh. Eksp. Teor. Fiz. **47**, 445 (1988) [JETP Lett. **47**, 526 (1988)].
[3] M.L. Du and J.B. Delos, Phys. Rev. A **38**, 1896 (1988); **38**, 1913 (1988).
[4] G. Alber, Z. Phys. D **14**, 307 (1989).
[5] A. Holle, G. Wiebusch, J. Main, B. Hager, H. Rottke, and K.H. Welge, Phys. Rev. Lett. **56**, 2594 (1986).
[6] G.R. Welch, M.M. Kash, C. Iu, L. Hsu, and D. Kleppner, Phys. Rev. Lett. **62**, 893 (1989); C. Iu, G.R. Welch, M.M. Kash, L. Hsu, and D. Kleppner, *ibid.* **63**, 1133 (1989).
[7] H. Friedrich and D. Wintgen, Phys. Rep. **183**, 37 (1989) and references therein.
[8] D. Delande, A. Bommier, and J.C. Gay, Phys. Rev. Lett. **66**, 141 (1991).
[9] J.M. Mao and J.B. Delos, Phys. Rev. A **45**, 1746 (1992).
[10] M.V. Berry and K.E. Mount, Rep. Prog. Phys. **35**, 315 (1972).
[11] J.N.L. Connors, Mol. Phys. **26**, 1217 (1973).
[12] Yu.A. Kravtsov and Yu.I. Orlov, *Geometrical Optics of Inhomogeneous Media* (Springer, Berlin, 1990).
[13] T. Poston and I.N. Stewart, *Catastrophe Theory and its Applications* (Pitman, London, 1978).
[14] J. Gao, J.B. Delos, and M. Baruch, Phys. Rev. A **46**, 1449 (1992); J. Gao and J.B. Delos, *ibid.* **46**, 1455 (1992).